Manuscript presented at the 10th MICCAI Workshop on Augmented Environments for Computer-Assisted Interventions (AE-CAI 2015), and published in Lecture Notes in Computer Science, vol. 9365, pp. 38-49, 2015.
DOI:10.1007/978-3-319-24601-7_5.
The final version of the paper is available at:
http://link.springer.com/chapter/10.1007/978-3-319-24601-7_5

3D Catheter Tip Tracking in 2D X-ray Image Sequences Using a Hidden Markov Model and 3D Rotational Angiography

Pierre Ambrosini[1], Ihor Smal[1], Daniel Ruijters[2], Wiro J. Niessen[1,4], Adriaan Moelker[3], and Theo van Walsum[1]

[1] Biomedical Imaging Group Rotterdam,
Department of Radiology and Medical Informatics,
Erasmus MC, Rotterdam, The Netherlands
p.ambrosini@erasmusmc.nl
[2] Philips Healthcare, Interventional X-ray Innovation, Best, The Netherlands
[3] Department of Radiology, Erasmus MC, Rotterdam, The Netherlands
[4] Imaging Science and Technology, Faculty of Applied Sciences,
Delft University of Technology, Delft, The Netherlands

Abstract. Integration of pre- or peri-operative images may improve image guidance in minimally invasive interventions. In abdominal catheterization procedures such as transcatheter arterial chemoembolization, 3D pre-/peri-operative images contain relevant information, such as complete 3D vasculature, that is not directly available from 2D imaging. Accurate knowledge of the catheter tip position in 3D is currently not available, and after registration of 3D information to 2D images (angiographies), the registration is invalidated by breathing motion and thus requires continuous updates. We propose a hidden Markov model based method to track the 3D catheter position, using 2D fluoroscopic image sequences and a 3D vessel tree obtained from 3D Rotational Angiography. Such a tracking facilitates display of the catheter in the 3D anatomy, and it enables to use the 3D vessels as a roadmap in 2D imaging. The tracking is initialized with the first 2D image of the sequence. For the subsequent images, based on a state transition probability distribution and the registration observations, the catheter tip position is tracked in the 3D vessel tree using registrations to the 2D fluoroscopic images. The method is evaluated on simulated data and two clinical sequences. In the simulations, we obtain a median tip position accuracies up to 2.9 mm. On clinical sequence, the distance between the catheter and the projected vessels after registration is below 1.9 mm.

Keywords: Catheter, Tip, Tracking, Rigid, Registration, Guidance, X-ray, Fluoroscopy, 3DRA, hidden Markov Model, Abdominal, TACE, Liver, Breathing

1 Introduction

Minimally invasive procedures are commonly performed to treat various diseases because they are less demanding and risky for the patient than, for example, open

surgeries. In such procedures, as direct eyesight is lacking, physicians require intra-operative images to visualize the instruments and the anatomy. During catheterization interventions, 2D fluoroscopic (X-ray) imaging is usually used, but the noise, 2D projection and inability to continuously use contrast agent prevent physicians to have a continuous understanding of the instrument position with regard to the 3D vasculature.

The purpose of our work is to improve image guidance in 2D X-ray guided sequence abdominal catheterization procedures, specifically during transcatheter arterial chemoembolization (TACE) procedures, by using 3D information from peri/pre-operative images. During the procedure, the physician injects chemotherapeutic agents and embolizes liver tumors by inserting a catheter into the femoral artery and guiding it toward the tumors. The physician uses single-plane 2D X-ray images in which only the catheter and the ribs are visible (Fig. 1). Pre-operative 3D Computed Tomography Angiography (CTA) and intra-operative 2D angiographies (X-rays with contrast agent) are acquired, providing detailed images of the arterial tree, and enabling a roadmap to guide the catheter. However, such static roadmaps are hampered by breathing motion and catheter deformation. We therefore propose a 3D tracking method that follows the position of the catheter tip in the 3D vessel tree, enabling guidance in the 3D image as well as facilitating continuous roadmapping.

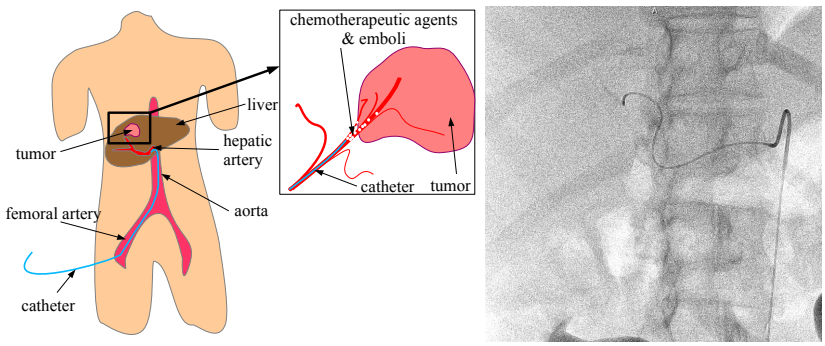

Fig. 1. TACE overview (left) and fluoroscopy example (right).

Image fusion and 3D/2D registration have already been addressed in the literature (see reviews [5, 7]), particularly for 2D X-ray guidance in cranial [8], cardiac [10] and abdominal [3] interventions. These methods rely on anatomical structures such as bones or the vasculature. A vessel-based rigid or non-rigid registration is done between pre-/peri-operative 3D images and single/bi-plane 2D angiographies or 2D fluoroscopies. These approaches align the 3D vessels with the 2D vasculature visualized using contrast agent. Such approaches cannot be used continuously because of the toxic nature of the contrast agent. Without contrast agent, in cardiac interventions, Ma et al. [6] use features such as diaphragm/heart border, tracheal bifurcation or the catheter to correct for breathing motion. In

2D abdominal fluoroscopies, however, such features are lacking. Other methods propose 3D/2D registration with peri-operative 3D Rotational Angiographies (3DRA) or Cone Beam Computed Tomography (CBCT) [1,2,11] where the calibrated geometry of the C-arm enables accurate alignment with the 2D X-ray images (acquired with the same device). Such an approach is effective in cranial interventions, as the head does not deform [11], but in abdominal procedures, the breathing motion invalidates the alignment. That is why a semi-automatic method following a region of the catheter [2] and a catheter-based registration [1] have been proposed to follow the catheter. Ambrosini et al. [1] have an automatic registration but when the catheter visible part is too short, the alignment fails. Position tracking of catheters has been addressed less frequently. The method proposed by van Walsum et al. [13] is one of the first approaches for neural applications.

In our work, we combine a hidden Markov model (HMM) [9] with 3D/2D registration to track the catheter tip in 3D over the time. The main contribution is a novel method for tracking the catheter tip in 3D, using a 3D vessel tree, 2D images and a HMM. The method is evaluated using a large set of simulated catheter motions in patient 3D datasets, and demonstrated on two patient cases.

2 Method

The purpose of our method is to track the catheter tip inside a 3D vessel tree, where the catheter position in 2D is obtained from the interventional X-ray images. As the catheter is assumed to be in the vasculature tree and as its displacement is relatively small between subsequent 2D images, we propose to model the catheter motion within the 3D vessel tree using hidden Markov model (HMM) [9]. Each 3D point of the vessel centerlines represents a state that denotes the probability that the catheter tip is at that location. Each state is linked with state transitions between connected close-by vessel parts. The observations to update the HMM are based on a 3D/2D registration metric where the 3D vessel tree is aligned with the 2D catheter visible in the image.

In the following, we explain the HMM, followed by a description of how the different elements of the HMM are integrated in our 3D tracking method.

2.1 Hidden Markov model

A HMM is described as a system with a set of states $S = \{s_1, \dots s_N\}$ (Fig. 2). The HMM changes, at each time point t, according to the probabilities associated with the states and the current set of observation $O_t = \{O_t(1), \dots O_t(N)\}$. The transition probabilities between states are defines in a matrix A (with a $N \times N$ dimension) where each $a_{ij} \in A$ is the probability that the state i can move to the state j ($a_{ij} \geq 0$ and $\sum_j a_{ij} = 1$).

Following Rabiner et al. [9], the Viterbi algorithm selects at time t the most probable path through the state space based on the maximum $\delta_t(i)$ which is the

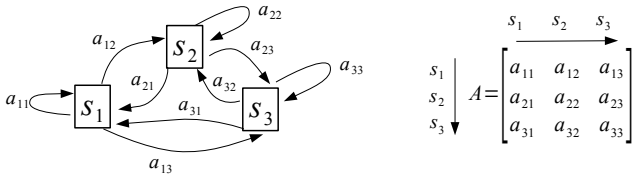

Fig. 2. HMM with 3 states and its matrix A of state transition probabilities.

best score (highest probability) along a single path that ends in state s_i. Viterbi takes into account the first t observations. Starting from an initial distribution of the probabilities over the states $\pi = \{\pi_1, \dots \pi_N\}$ where $\sum_{j=1}^{N} \pi_j = 1$, the algorithm initializes the $\delta_1(i)$ as follows:

$$\delta_1(i) = \pi_i \cdot O_1(i) \quad ,$$

where $O_1(i)$ is an observation score given that we are in the state s_i at time $t = 1$. Next, the subsequent $\delta_t(i)$ can be computed using recursion:

$$\delta_t(j) = \max_i [\delta_{t-1}(i) \cdot a_{ij}] \cdot O_t(j) \quad .$$

2.2 Catheter tip tracking

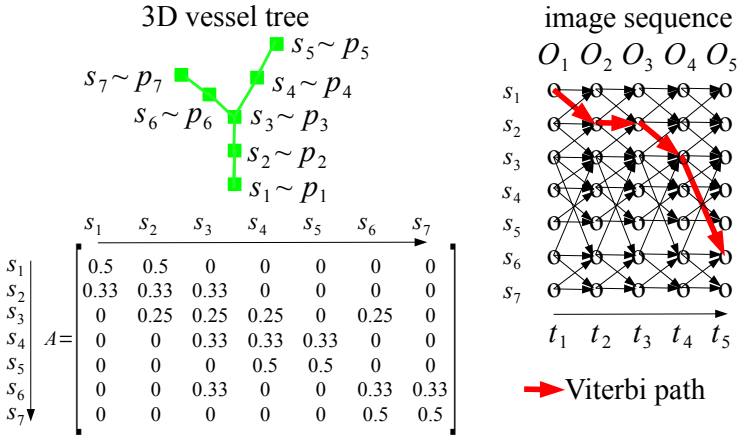

Fig. 3. HMM with a simple vessel tree. Here, the transitions between possible tip locations exist only with direct neighbours and are equiprobable. The Viterbi path goes to the optimum tip position knowing the observations $O_1 \dots O_5$ in the 5-images sequence.

Timepoint and states At each timepoint t, a single 2D fluoroscopic image of the complete image sequence is processed. In this image, the 2D catheter centerline $C_t = \{c_1, \dots c_{n_C}\}$ is extracted, where c_1 is the tip of the catheter. The full 2D catheter is used during the 3D/2D registrations to compute the observations. A set of 3D points $P = \{p_1, \dots p_N\}$, corresponding to the 3D vessel centerlines, is extracted from the peri-operative 3DRA. In the HMM, the probability of being in state s_i is the probability of the catheter tip being at position p_i (Fig. 3).

Matrix *A* of state transition probabilities Each a_{ij} in the matrix A contains the probability that the catheter tip moves from the position p_i to p_j (state s_i to s_j) between two images. In the context of tip motion, the closer p_i and p_j are, the higher the probability of transition should be.

To define A, the transition probabilities are set according to the distance along the vessel path between points p_i and p_j of the 3D vessel tree and distributed with a Gaussian function:

$$a_{ij}^{'} = e^{-\frac{D(p_i,p_j)^2}{2\sigma_a^2}}$$

where σ_a controls how far the catheter tip can move. If $\{l_1, \dots l_n\}$ is the set of points representing the vessel centerline between the points $p_i = l_1$ and $p_j = l_n$, $D(p_i, p_j)$ is defined as the sum of the distances between each neighboring pair l_k, and l_{k+1}:

$$D(p_i, p_j) = \sum_{k=1}^{n-1} ||l_k, l_{k+1}|| \quad .$$

Because the matrix A defines probabilities, $\sum_j a_{ij}$ has to be equal to 1 so we normalize the coefficients to obtain $a_{ij} = a_{ij}^{'} . (\sum_j a_{ij}^{'})^{-1}$.

Observations An observation score $O_t(i)$, under the assumption that the catheter tip is at the position p_i (thus in the state s_i), has to be determined. From the 3D vessel tree, the unique 3D catheter path centerline $V_i = \{v_1, \dots v_{n_V}\}$, starting from the tip p_i and going to the root of the tree, is extracted. This 3D path V_i is registered to the current 2D catheter C_t, obtaining a rigid transformation that aligns the 3D vessel tree with the catheter centerline in the 2D image. The observation score $O_t(i)$ (between 0 and 1) using the metric M of the 3D/2D registration is defined as follows:

$$O_t(i) = e^{-\frac{M(C_t,V_i)^2}{2\sigma_s^2}}$$

where σ_s controls the registration score distribution and where M is defined as the minimum sum of the minimal distance between each point of the 2D catheter

C_t and any projected point of the 3D centerline V_i:

$$M(C_t, V_i) = \min_{\tau} \left(\sum_{c \in C_t} \min_{v \in V_i} ||c - F_{\text{proj}}(v, \tau)|| \right)$$

where $F_{\text{proj}}(v, \tau)$ is the projection of the 3D point v onto the 2D images and τ represents a 4 degrees of freedom rigid transformation matrix (three rotations and one translation) used to align the catheter C_t and the vessel path V_i. We define the projection function F_{proj} as follows (Fig. 4):

$$F_{\text{proj}}(v, \tau) = T_{\text{proj}}.T_{\text{det} \leftarrow w}.T_{w \leftarrow l_i}.\tau.T_{l_i \leftarrow w}.T_{\overrightarrow{p_i l_i}}.v$$

where T_{proj} is the cone-beam projection and $T_{\text{det} \leftarrow w}$ the transformation matrix from the C-arm world to the detector (X-ray image plane). Both transformations are known because of the C-arm geometry (given in the DICOM file). As the projection of the 3D tip p_i has to match the 2D catheter tip c_1 (i.e. $F_{\text{proj}}(p_i, \tau) = c_1$), the search of the transformation τ translates along the line from c_1 to the origin of the X-ray projection and rotates around it (Fig. 4). l_i is the intersection point of the projection line of c_1 and the plane, containing p_i, parallel to the patient table. It is a coherent starting point for the registration search because we are expecting mostly only a breathing motion of p_i in the cranial-caudal direction. τ is thus computed in the coordinate system around l_i. $T_{\overrightarrow{p_i l_i}}$ is the in-plane translation from p_i to l_i in the world coordinate system.

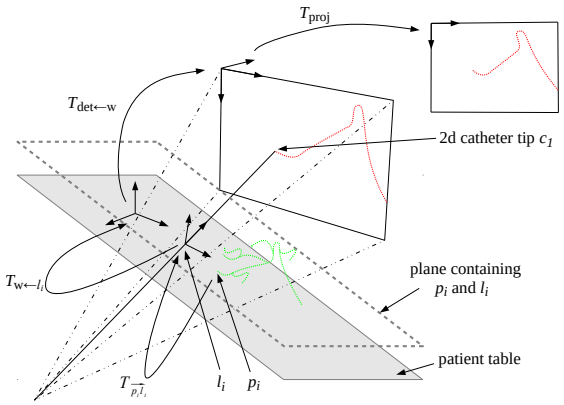

Fig. 4. Transformations in the projection function F_{proj}.

Viterbi For each image in the sequence, using the Viterbi algorithm [9], the Viterbi path (best tracking of the tip) is computed from the initial state position at the first image to the current image. The result gives the highest probability

of the 3D tip position p_i and also (as a 3D/2D registration has been performed during the observations computations) the transformation τ to align the 3D vessel tree inside the 2D fluoroscopy.

3 Experiments and Results

We perform two experiments. First, we evaluate the accuracy of the catheter tip tracking using clinical image data where the catheter and the breathing motion are simulated. In these experiments, the availability of the ground truth from the simulation permits quantitative evaluation. Next, we demonstrate the approach for tip tracking on two real image sequences.

3.1 Implementation

We retrospectively acquired anonymized data of 19 TACE procedures in three different hospitals using intervention rooms with angiographic C-arm systems (Xper Allura, Philips Healthcare, Best, the Netherlands). In total, we acquired 67 fluoroscopic image sequences. A 3DRA was acquired at the beginning of each intervention when the catheter was in the hepatic artery. The 2D catheter is manually segmented in each fluoroscopic image and the 3D vessel tree in the 3DRA is extracted with a semi-automatic method based on thresholding and skeletonization [12].

The matrix A of state transition probabilities is built with $\sigma_a = 12$ mm which enables a relatively large catheter tip motion per frame. The registration score uses $\sigma_s = 1.5$ mm, which penalizes registrations where the normalized sum of the minimal distance $M(C_t, V_i)$ is larger than 1.5 mm. These values have been chosen after a pilot on one simulated image sequence. For the initialization, $\delta_1(i)$ is equal to 1 in the state where the tip is and equal to 0 for all the other states. We manually initialize the tip position of the first image of each sequence. The discretization of the 3D blood vessel and the 2D catheter are set to 3 mm. Because the method has to be computed in real-time, the number of observations $O_t(j)$ to compute at time t is limited to 50. Thus, to calculate every $\delta_t(j)$, we sort in descending order the states s_j based on the probabilities $\max_i[\delta_{t-1}(i) \cdot a_{ij}]$ and compute the observations $O_t(j)$ for the 50 first states s_j in the sorting. All the other state observations are assumed to return a score close to 0, as those states have very low probabilities. Therefore these observation scores are set directly to 0 without any computation and thus δ_t will be also 0. When we compute the observation scores, $M(C_t, V_i)$ is minimized using the Powell optimizer to find the 4 degrees of freedom rigid transformation matrix τ. The search space is limited to $\pm 2^\circ$ for the three rotations and ± 2 mm for the translation along the projection line. The average computation time for each image is below 60 ms with a 2.0Ghz Intel Core i7 processor.

3.2 Clinical data with a simulated catheter and breathing motion

As we do not have ground truth for the catheter position in 3D in our clinical data, we evaluate our method on simulated data. We use the 3D vessel tree from the 3DRA and also the projection geometry of the fluoroscopic images sequence (saved in the DICOM file). Initially, the catheter tip is positioned at a proximal location in the 3D vessel tree, and over time the tip is advanced. The catheter shape in 3D is obtained by smoothing the corresponding vessel centerline with a Gaussian kernel. The effect of liver motion due to respiration is simulated with a translation along the y-axis (cranial-caudal direction), where the translation magnitude is defined as:

$$translation_y(i) = \lambda \cdot \sin(\frac{2\pi}{\beta} \cdot i \cdot \Delta_t - \frac{\pi}{2})$$

where $\lambda = 10$ mm is the peak amplitude, $\beta = 4$ s the respiration period, i the number of the current image in the sequence and $\Delta_t = 0.133$ s the time between two images, obtained from the fluoroscopic image frequency.

The simulated catheter tip has three different constant speeds: 1.5, 3 and 6 mm/frame (resp. 11.2, 22.5 and 45 mm/s), which is similar to tip speeds during clinical procedures. The simulation has two catheter deformations: slight (Gaussian smoothing with a random (between each image sequence) $\sigma \in [3, 6]$ mm) and large ($\sigma \in [7, 11]$ mm). We tracked the tip and registered all the 67 simulated sequences starting with the correct initial registration at the first frame.

To evaluate the tip tracking, we compute the distance between the real tip and the registered tip chosen by the HMM at every image frame. Both the distance in the 2D image space and the 3D world space are calculated. The average distances between the real 2D projected tip and the registered 2D projected tip for every simulated sequence with different tip speeds and catheter deformations are presented in Figure 5. The medians of the distances are in a range of 1.1 and 2.7 mm. These distances increase when the deformation is larger and also when the tip moves faster. The average distances between the real 3D tip and the registered 3D tip for every simulated sequence with different tip speeds and catheter deformations are also shown in Figure 5. The medians of the tip distances are up to 2.9 mm. We define an incorrect tip tracking when the distance between the real 3D tip and the registered 3D tip, in the last 5 images of a tracked sequence, is superior to 3 mm. Following this definition, Table 1 shows the percentage of sequence in which the tracking is incorrect at the end of the sequence. This percentage is up to 7.8%.

3.3 Clinical data

We applied the method on two clinical sequences. As there is no ground truth for the 3D tip position available, we qualitatively evaluated whether the tracking is consistent. In these sequences, the catheter tip is moved from the hepatic artery to a vessel close to the tumor. The first frame is manually registered and

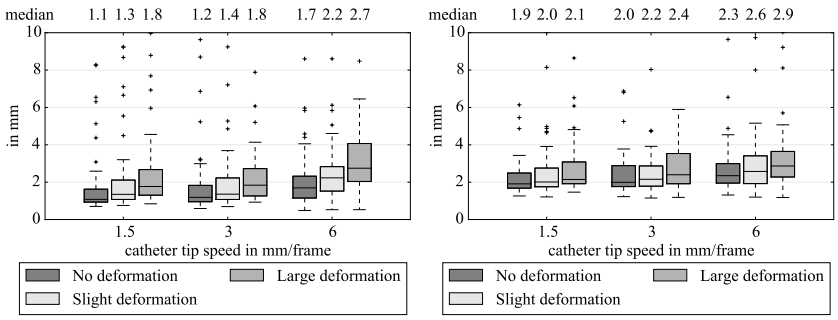

Fig. 5. Average distance for each sequence between the real 2D projected tip and the registered one with different simulation parameters (left). Average distance for each sequence between the real 3D tip and the registered one (right).

Table 1. Percentage of incorrect tip tracking at the end of the sequences with different simulation parameters.

catheter tip speed	no deformation	slight deformation	large deformation
1.5 mm/frame	7.8%	6.2%	7.8%
3 mm/frame	4.7%	1.6%	0.0%
6 mm/frame	3.1%	3.1%	1.6%

the method is run on the sequences (74 frames each at 7.5 Hz). Visual checking showed that the registration is approximately correct. Video clips showing the tracking on both sequences are available as supplementary material. In the second sequence, at a bifurcation, the tip goes in the wrong vessel but goes back to the correct one after two frames. We also computed the distance from each catheter point (in 2D) to the closest point of the projected centerline V_i after registration (see Figure 6). For both sequences, the average point distances between the catheter and the vessel V_i are below 1.9 mm. Figure 7 shows one registered frame of the first sequence.

4 Discussion and conclusion

We proposed a method for tracking the 3D catheter tip in fluoroscopies using an HMM and registration with the 3D vessel tree extracted from a 3DRA. The method uses the Markov models to estimate the probabilities of the states, which represent the possible catheter tip positions in the 3D vessel tree. The evaluation on simulated data showed a median distance between the real tip and the registered one up to 2.7 mm in the 2D image space and up to 2.9 mm in the 3D space. With the two clinical sequences, we obtain an average distance between the 2D catheter centerline and the projection of the 3D vessel centerline below 1.9 mm.

As the discretization of the catheter centerline and the blood vessel tree is 3 mm, the distances between real tip and registered tip are close to the sampling.

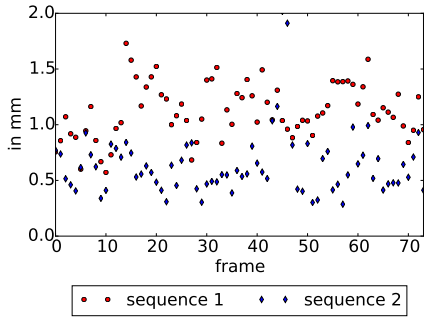

Fig. 6. Average distance (in mm), of the clinical sequences, between points from the 2D catheter centerline and their closest points from the 2D projected vessel centerline V_i, after registration at each frame.

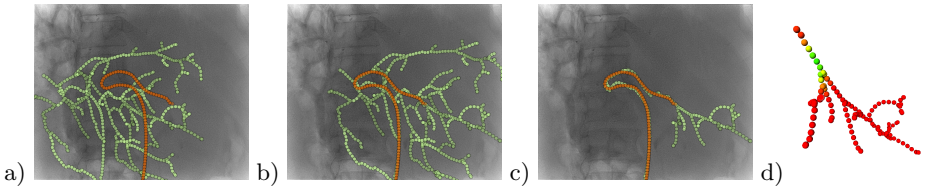

Fig. 7. Tip tracking with 2D catheter (in orange) and 3D vessel tree projection (in green). Before the tracking (a), breathing and table motion prevent the alignment. After the tracking, the roadmap is possible with all the vessel tree visible (b) or only the vessels after the tracked tip (c). Close view of the 3D tracking tip score δ_t inside the vasculature (d) with a colored scale: red (score = 0) to green (score = best score).

The tracking gives better tip accuracy when the motion of the catheter is small and the catheter deformation is slight. The percentage of incorrect tracking at the end of the sequence (up to 7.8%) is relatively low and is not impacted by deformation. It is higher for the slow catheter motion which implies that the parameter σ_a for the state transition matrix A is probably too large for static and slow catheter motion.

Evaluation of the method on the two clinical cases showed that the catheter and the 3D vessel tree match well. According to our clinical partners, the tracking of the tip position (both in 2D and 3D) is accurate enough to be used for roadmapping and to provide the physician with an overview of where the catheter is and where to go.

Robust automatic 2D catheter segmentation is required after initialization to integrate our method into the interventional workflow. Heibel et al. [4] obtained a mean error of real-time catheter tracking less than 1.2 pixels for abdominal fluoroscopies. Those results should be sufficiently accurate for our registration. In clinical practice, the first initialization of the catheter tip position can be done after the 3DRA acquisition by pointing the catheter tip in the 3DRA. Due to clear visibility of the catheter, this task could be easily automated.

The lack of a ground truth position of the catheter in 3D hampers thorough evaluation of approaches such as ours, which is why we employed extensive experimentation using simulated catheter positions obtained from clinical patient data. Additionally, qualitative evaluation was performed using clinical data only, demonstrating that the method is able to consistently track the position in 3D.

Whereas we have now fixed the parameter σ_a for the state transition matrix A, and the σ_s for converting the registration distance to an observation score, based on a pilot experiment, these values could be tuned to a specific patient or anatomy (e.g. at bifurcations). In the future we therefore intend to investigate the impact of these parameters and how they should be set optimally for each case.

To conclude, we have presented a model to track a catheter tip thanks to 2D fluoroscopies and 3DRA. We evaluated the feasibility of our approach with simulated data demonstrating a tip accuracy below 2.7 mm in 2D image space and 2.9 mm in 3D space. The method was also successfully applied in two clinical cases.

Acknowledgement. This research is funded by Philips Healthcare, Best, The Netherlands.

References

1. Ambrosini, P., Ruijters, D., Niessen, W.J., Moelker, A., van Walsum, T.: Continuous roadmapping in liver tace procedures using 2d–3d catheter-based registration. International Journal of Computer Assisted Radiology and Surgery pp. 1–14 (2015)
2. Atasoy, S., Groher, M., Zikic, D., Glocker, B., Waggershauser, T., Pfister, M., Navab, N.: Real-time respiratory motion tracking: roadmap correction for hepatic

artery catheterizations. In: Medical imaging. pp. 691815–691815. International Society for Optics and Photonics (2008)
3. Groher, M., Zikic, D., Navab, N.: Deformable 2d-3d registration of vascular structures in a one view scenario. Medical Imaging, IEEE Transactions on 28(6), 847–860 (2009)
4. Heibel, H., Glocker, B., Groher, M., Pfister, M., Navab, N.: Interventional tool tracking using discrete optimization. Medical Imaging, IEEE Transactions on 32(3), 544–555 (2013)
5. Liao, R., Zhang, L., Sun, Y., Miao, S., Chefd'Hotel, C.: A review of recent advances in registration techniques applied to minimally invasive therapy. IEEE transactions on multimedia 15(5), 983–1000 (2013)
6. Ma, Y., King, A.P., Gogin, N., Gijsbers, G., Rinaldi, C., Gill, J., Razavi, R., Rhode, K.S.: Clinical evaluation of respiratory motion compensation for anatomical roadmap guided cardiac electrophysiology procedures. Biomedical Engineering, IEEE Transactions on 59(1), 122–131 (2012)
7. Markelj, P., Tomaževič, D., Likar, B., Pernuš, F.: A review of 3d/2d registration methods for image-guided interventions. Medical image analysis 16(3), 642–661 (2012)
8. Mitrović, U., Spiclin, Z., Likar, B., Pernuš, F.: 3d-2d registration of cerebral angiograms: a method and evaluation on clinical images. Medical Imaging, IEEE Transactions on 32(8), 1550–1563 (2013)
9. Rabiner, L.: A tutorial on hidden markov models and selected applications in speech recognition. Proceedings of the IEEE 77(2), 257–286 (1989)
10. Rivest-Henault, D., Sundar, H., Cheriet, M.: Nonrigid 2d/3d registration of coronary artery models with live fluoroscopy for guidance of cardiac interventions. Medical Imaging, IEEE Transactions on 31(8), 1557–1572 (2012)
11. Ruijters, D., Homan, R., Mielekamp, P., Van de Haar, P., Babic, D.: Validation of 3d multimodality roadmapping in interventional neuroradiology. Physics in medicine and biology 56(16), 5335 (2011)
12. Selle, D., Preim, B., Schenk, A., Peitgen, H.O.: Analysis of vasculature for liver surgical planning. Medical Imaging, IEEE Transactions on 21(11), 1344–1357 (2002)
13. Van Walsum, T., Baert, S.A., Niessen, W.J.: Guide wire reconstruction and visualization in 3dra using monoplane fluoroscopic imaging. Medical Imaging, IEEE Transactions on 24(5), 612–623 (2005)